Journal of Natural Gas Science and Engineering 51 (2018) 129–140

Contents lists available at ScienceDirect

Journal of Natural Gas Science and Engineering

journal homepage: www.elsevier.com/locate/jngse

Reconstruction of 3D porous media using multiple-point statistics based on a 3D training image

Yuqi Wu[a], Chengyan Lin[a,*], Lihua Ren[a], Weichao Yan[a], Senyou An[b], Bingyi Chen[a], Yang Wang[a], Xianguo Zhang[a], Chunmei You[c], Yimin Zhang[a]

[a] School of Geosciences, China University of Petroleum (East China), Qingdao, China
[b] Research Centre of Multiphase Flow in Porous Media, China University of Petroleum (East China), Qingdao, China
[c] Exploration and Development Research Institute of Daqing Oilfield Limited Company, Daqing, China

ARTICLE INFO

Keywords:
Porous media
Multiple-point statistics
Training image
Pore network model
Berea sandstone

ABSTRACT

To date many methods of constructing porous media have been proposed. Among them, the multiple-point statistics (MPS) method has a unique advantage in reconstructing 3D pore space because it can reproduce pore space of long-range connectivity. The Single Normal Equation Simulation (SNESIM) is one of most commonly used algorithms of MPS. In the SNESIM algorithm, the selection of training image is vital because it contains the basic pore structure patterns. In the previous reconstructions of 3D porous media using SNESIM, a 2D slice was usually employed as the training image. However, it is difficult for a 2D slice to contain complex 3D pore space geometry and topology patterns. In this paper, a 3D training image is used in order to provide more realistic 3D pore structure features. Besides, a multi-grid search template is applied for the purpose of capturing the pore structures of different scales and speeding up the reconstruction process. Two sandstone cores are taken as test examples and the 3D porous media are reconstructed. The two-point correlation function, pore network structure parameters and absolute permeability are applied as the evaluation indexes to validate the accuracy of the reconstructed models. The comparison result shows that the reconstructed models are in good agreement with the real model obtained by X-ray computed tomography scanning in the pore throat geometry and topology and transport property, which justifies the reliability of the proposed method.

1. Introduction

Porous media modeling—pore-scale imaging and modeling is becoming more and more popular for engineers of both petroleum and environment fields to predict the macroscopic transport properties and understand the displacement processes (Blunt et al., 2013; Wang et al., 2007; Chen and Zhou, 2017; Chen and Yao, 2017; Chen et al., 2016; Abdelfatah et al., 2017; Alizadeh et al., 2014; An et al., 2016a; Kakouei et al., 2017; Vaz et al., 2016). As a result, a new technique, digital rock analysis, has been developed not only for understanding the visualization of pore structures and mineral spatial arrangement (Chen and Zhou, 2017; Liu et al., 2016), but also for predicting various petrophysical properties and studying transport processes, such as transport of electricity, acoustic wave and multiphase flow in porous medium (Van der Land et al., 2013; Wang and Chen, 2007; Arabjamaloei and Ruth, 2016; An et al., 2016b; Nooruddin and Blunt, 2016; Qajar and Arns, 2016; Liu et al., 2017). In essence, these transport properties are governed by the types of grains, the morphology and topology of the pore space, arrangements between the grains and pore space and the conditions of transport process (Okabe and Blunt, 2005; Tahmasebi and Sahimi, 2012). The premise of predicting these properties and understanding these transport processes is to build an accurate 3D pore space.

With the innovation of experimental instruments and the breakthrough of new theories, scholars have put forward many methods to construct the porous media. So far, the methods of modeling porous media are divided into two main groups, namely, experiment technology methods and statistical methods. The former applies experimental instruments to photograph or scan the rock sample to obtain a large number of 2D images, then uses the software to build a 3D rock model by stacking these 2D slices. For this approach, X-ray computed tomography (Blunt et al., 2013, An et al., 2016a), focused ion beams (Hemes, et al., 2015; Kim et al., 2012) and laser scanning confocal microscopy (Minsky, 2011; Paddock, 2000) are common tools. Although the X-ray computed tomography scanning method and focused ion beams can establish an accurate 3D digital core model, they are so expensive and time-consuming (Hajizadeh et al., 2011). Statistical

* Corresponding author.
E-mail address: ycdzycmsi@126.com (C. Lin).

https://doi.org/10.1016/j.jngse.2017.12.032
Received 11 September 2017; Received in revised form 27 November 2017; Accepted 28 December 2017
Available online 11 January 2018

methods employ stochastic algorithms to generate stochastic models based on the little information from the slices. These methods include the truncated Gaussian random field (Quiblier, 1984; Ioannidis et al., 1997; Yeong and Torquato, 1998), simulated annealing (Talukdar and Torsaeter, 2002 ; Talukdar et al., 2004; Kainourgiakis et al. 2005; Ju et al. 2014), Markov chain Monte Carlo (Wu and Crawford, 2004; Wu et al., 2006), sequential indicator simulation (Keehm, 2003; Keehm et al., 2004), multiple-point statistics (Okabe and Blunt, 2004; Okabe and Blunt, 2005; Tahmasebi et al., 2012; Comunian et al., 2012; Xu et al., 2012; Hurley et al., 2015; Tahmasebi et al., 2015a; Tahmasebi et al., 2015b), phase-recovery algorithm (Fullwood et al., 2008; Hasanabadi et al., 2016a; Hasanabadi et al., 2016b) and process-based or grain method (Øren and Bakke, 2002; Øren and Bakke, 2003; Biswal et al., 2007; Thovert and Adler, 2011). Comparing with the former method, the latter not only has the merits of low cost and high efficiency, but it can also combine different scale information and reconstruct a larger model (Blunt et al., 2013). However, the truncated Gaussian random field, simulated annealing and sequential indicator simulation rely on the variogram to evaluate the correlation of two points of the geological variable. The variogram is difficult to precisely simulate the void space with complex geometry and topology, which tends to cause reconstruction of the pore space lacking of long-range connectivity (Hajizadeh et al., 2011; Tahmasebi and Sahimi, 2012; Tahmasebi et al., 2012). In 2002, Bakke and Øren put forward a new modeling technique based on the formation of sedimentary rock containing sedimentation, compaction and diagenesis processes (Øren and Bakke, 2002). But the process-based method assumes that all the particles are spheres, which is not real for the sedimentation of grains in that the shape of most grains is irregular when they are depositing. The method also only simulates several diageneses, such as quartz cement overgrowth and clays growth, so it is not suitable for simulating the rock of having undergone complex diageneses. The above disadvantages have contributed to the proposal of a more accurate method based on the multiple-point statistics (MPS) that can effectively address the aforementioned problems especially in the long-range connectivity (Deutsch, 1992; Strebelle, 2000; Strebelle, 2002; Okabe and Blunt, 2004; Okabe and Blunt, 2005; Tahmasebi et al., 2012; Comunian et al., 2012; Xu et al., 2012; Hurley et al., 2015).

MPS was first proposed by Deutsch (1992). To date MPS is divided into two major categories, iterative algorithms and noniterative algorithms (Strebelle, 2002). Iterative algorithms were extremely CPU demanding and seriously restricted the efficiency (Guardiano and Srivastava, 1993). Until 2000, Strebelle proposed the Single Normal Equation Simulation (SNESIM) algorithm that effectively overcomes the problem associated with the previous algorithm (Strebelle, 2000). SNESIM algorithm applies the search tree to record and store the conditional probability distribution of all data events acquired by scanning the training image, which needs to scan the training image only once in the simulation process and dramatically reduces the computational time needed.

MPS has been widely used in reservoir modeling (Srivastava, 1992; Liu, 2006; Boucher, 2009), especially in fluvial facies. In 2004, Okabe and Blunt reconstructed digital rock modeling using the MPS (Okabe and Blunt, 2004, 2005, 2007). They took a 2D image from 3D micro-CT data of the rock as the training image and rotated this image around each principal axis to generate 3D conditioning data. Then the preferred search template was used to scan the training image and a stochastic 3D digital rock was reconstructed. Comparing with the model established by the simulated annealing method, the curve fraction of percolating cells of the model gotten by MPS is in better agreement with the curve of the real model obtained by the X-ray computed tomography scanning, which verifies that MPS is better than the simulated annealing method in reproducing the pore space of long-range connectivity.

However, Okabe and Blunt assumed that the porous medium was explicitly isotropic in X, Y and Z directions, which is obviously unreal for the heterogeneous rock. Therefore, a novel idea was proposed to address the problem by generating a sequence of 2D slices and stacking these 2D slices. (Hajizadeh et al., 2011). Later, the cross-correlation simulation method was also presented to reconstruct anisotropic 3D digital rocks only using a single 2D thin section (Tahmasebi and Sahimi, 2012; Tahmasebi et al., 2015a, 2015b). Other scholars also reconstructed some 3D porous media based on a 2D training image (Comunian et al., 2012; Xu et al., 2012; Hurley et al., 2015). For these reconstructions, the training image is only one 2D slice. In fact, a 2D image cannot contain 3D pore-space structural features, for example the topology characteristic (Zhang, 2015). Different from the previous reconstruction of porous media using SNESIM algorithm, we will make use of a 3D training image built by X-ray computed tomography scanning taking the place of a 2D training image to supply the more accurate 3D pore structures in this paper. Two orthogonal slices are set to the conditioning data. That is, the Berea sandstone and S sandstone cores are taken as the test examples. For each porous medium, two representative volume elements (RVE) of 150^3 voxels from different locations are extracted. One is set for the 3D training image so as to provide more real pore space structure patterns, the other for the real model to supply the conditioning data and be compared with the next reconstructed models to validate the proposed method. Two orthogonal 2D slices are chosen from the real model, second RVE, as the conditioning data. The SNESIM algorithm is applied to generate the stochastic porous media through using the 3D training image and multigrid search template under the constraint of the conditioning data. This paper is organized as follows: Sections mainly gives a brief introduction of SNESIM algorithm including some terminologies while Section 3 describes modeling steps in detail and parameters setting. The evaluation of the accuracy of reconstructed models is going to be demonstrated in Section 4. Section 5 makes a summary of the full text.

2. SNESIM algorithm

SNESIM algorithm is one of the most common methods for discrete variable simulation in MPS, for example pore space (Tahmasebi et al., 2012). To facilitate the understanding of this algorithm, several important terminologies in the algorithm are briefly introduced below.

2.1. Data template and data event

Data template τ_n, as well as search template, consists of central node $\mathbf{u}$ and n vectors $\{\mathbf{u} + \mathbf{h}_\alpha, \alpha = 1,2, \cdots, n\}$ radiating from the center node. A data event d_n is constituted by the data template τ_n and the n data values of the n vectors $\{\mathbf{u} + \mathbf{h}_\alpha, \alpha = 1,2, \cdots, n\}$. A square 7×7 data template and a data event are shown in Fig. 1. In the digitized image, the node is usually substituted for the term “pixel” or “voxel” to represent a minimum unit in the paper. The pixel is used in 2D image and voxel is used in 3D image.

2.2. Training image

A training image is essentially a conceptual model that should try to include all pore structure patterns for porous media. The training image can be derived from the 3D model obtained by micro-CT machine, or from 2D slices such as cast thin sections or scanning electron microscope images. Fig. 2(a) exhibits a training image and Fig. 2(b) shows the training image scanned by a 7×7 search template. One of the key factors that affect the accuracy of reconstructed models is the selection of a training image. The size choice of a training image determines how much pore structure features the training image will contain. In terms of the theory, the simulation result will be better with the training image of larger size. But due to computer properties, such as the CPU, the choice of training images should be comprehensively considered (Liu, 2006). Moreover, the 3D training image should be preferred to 2D training image in that more real pore structures can be included in the

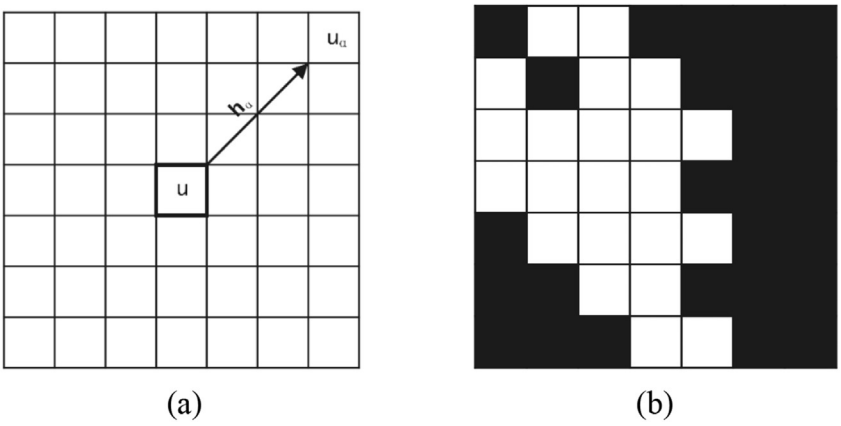

Fig. 1. (a) A 7 × 7 data template comprised of the central node **u** and 48 vectors $\{\mathbf{u} + \mathbf{h}_\alpha, \alpha = 1,2, \cdots, 48\}$ (b) A data event acquired after a 7 × 7 template scans the training image. The grain is demonstrated black, the pore space white.

3D image (Zhang, 2015).

2.3. Search tree

A search tree is a tree data structure comprised of a series of nodes. Each node on the tree represents a data event. The search tree is used to store and classify occurrences of all pore structure patterns that are obtained after the search template scans the training image. Fig. 3 displays the formation of a search tree. Such an efficient record facilitates directly reading the conditional probability distribution function (CPDF) from the search tree. It ensures that the reconstruction requires scanning the training image only once, so it can improve the modeling efficiency.

2.4. Multiple grid simulation

In the process of porous medium reconstruction, the size of the search template determines what size of the pore structure in the training image will be captured (Strebelle, 2002). In order to capture large-scale structure information, increasing the search template size often affects simulation efficiency. Therefore, a multiple grid template is applied to solve the problem so as to capture multi-scale pore structure information and improve the modeling efficiency. In the multiple grid, a multi-grid search template instead of a large and dense data template will be employed to scan the training image. During the simulation process, the large-scale structures are obtained by scanning the training images with coarse grid templates, then the simulated results of these coarse grid simulation are used as the conditioning data for the simulation of fine grids. Small-scale pore space structures are captured with fine grid templates. Define G^g as gth grid. In the gth grid, search template τ_n will be rescaled by 2^{g-1} factor such that

$$\tau_n^g = \{2^{g-1}h_\alpha, \alpha = 1,2,\cdots,n\} \quad (1)$$

where τ_n^g represents gth grid search template. Fig. 4 exhibits the schematic diagrams of a 3 multiple grid and a 3 multi-grid template.

3. Porous media reconstruction

For SNESIM algorithm, the core principle of reconstructing porous media is that the search template is used to scan the training image to obtain multi-scale structure patterns of pore space. The obtained pore structure patterns are stored in the search tree. Under the constraints of conditioning data, the CPDF of each unknown voxel is calculated and determined by retrieving corresponding patterns in the search tree. Based on the sequential simulation, the node values that have been simulated will be changed as the conditioning data for the next unknown voxel to be simulated. That this algorithm considers the relationship of multiple voxels on different scales with multi-grid template is its advantage, which makes it more suitable for reconstructing the pore space with long-range connectivity.

Different from the previous reconstruction of porous media using SNESIM algorithm, in our research, one 3D image is chosen as the training image to provide the 3D pore structure patterns, and two orthogonal slices from another 3D image are set to the conditioning data. Within the constraint of the conditioning data, some pore structure patterns are borrowed from the training image to constitute the new porous media with the hope that these generated porous media are similar to the second 3D image. The 3D training image is selected because it can contain 3D patterns of the pore structures, especially the topology features of the pore space.

For validating the proposed method, the Berea sandstone and S sandstone are selected as the test samples. The data of Berea and S porous samples have been collected by X-ray computed tomography scanning at Imperial College London, with the resolution of 5.345 μm and 9.1 μm respectively. Compared with the Berea sandstone, the S

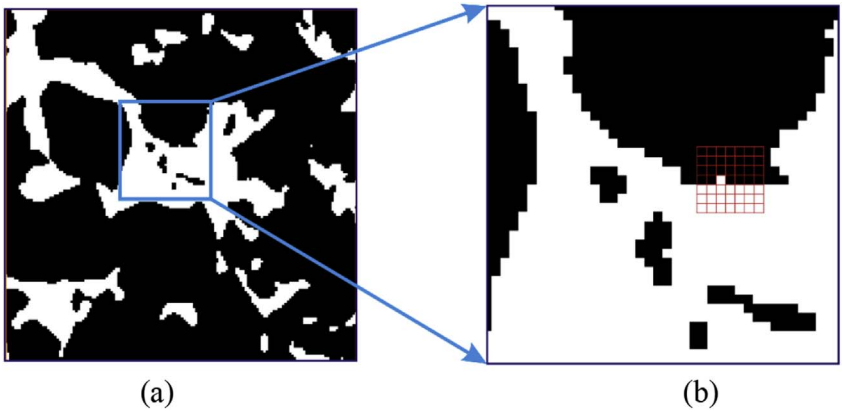

Fig. 2. Illustration of the training image scanned by a search template. The grain is demonstrated black, the pore space white. The resolution of the slice is 5.345 μm. (a) Training image is derived from a 2D slice of Berea sandstone with the size of 150 × 150 pixels. (b) The training image is scanned by a 7 × 7 search template shown red grids. (For interpretation of the references to colour in this figure legend, the reader is referred to the Web version of this article.)

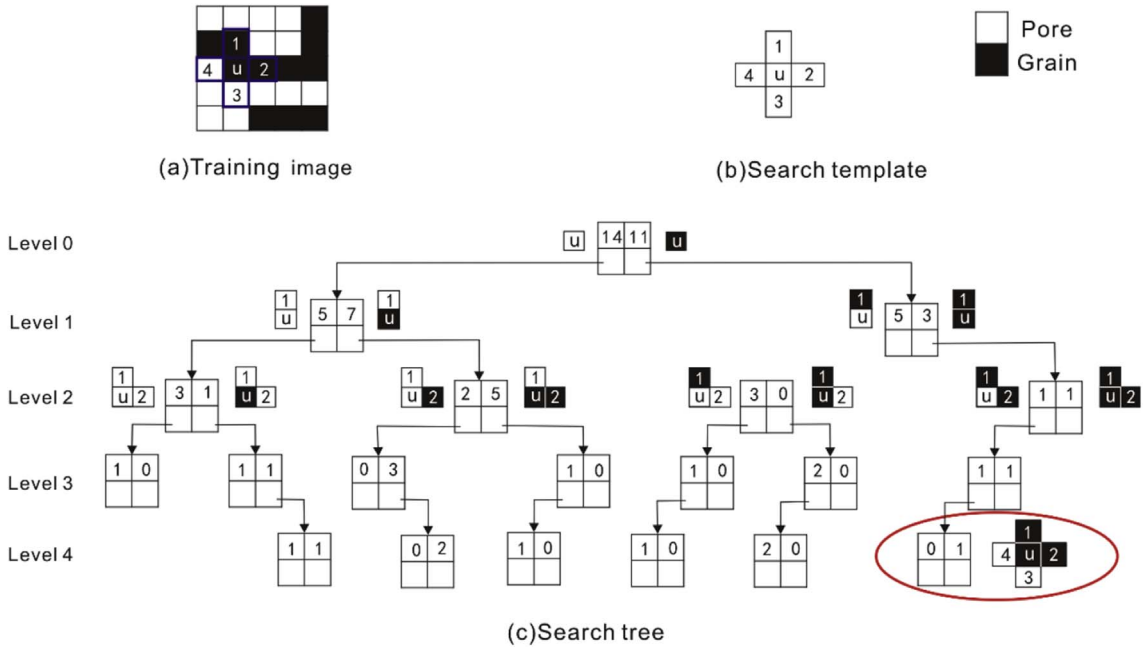

Fig. 3. Principle illustration of search tree. A search tree (c) is constructed by using the search template (b) to scan the training image (a). The probability of which **u** at the center of the data template in the level **0** is the pore is 14/25. The red oval of the level **4** represents that when the nodes 1 and 2 are solid and the nodes 3 and 4 are pore, the node **u** is the pore. (For interpretation of the references to colour in this figure legend, the reader is referred to the Web version of this article.)

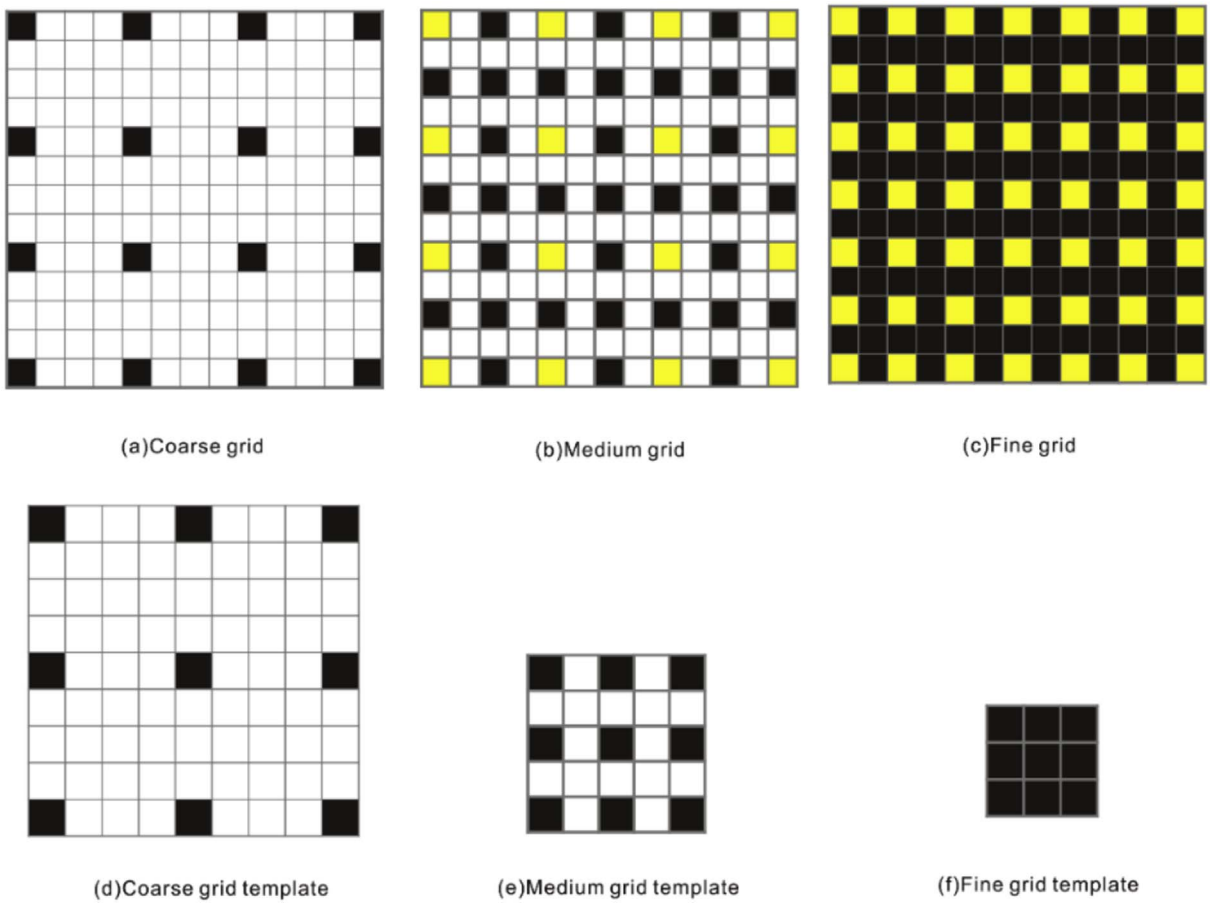

Fig. 4. A multiple grid (a, b and c) and corresponding multi-grid search template (d, e and f). The valid node is displayed black, the conditioning data yellow and the invalid node white that can be ignored. The values of black nodes of the coarse (1st) grid (a) are obtained by using the coarse grid search template. When the coarse grid is completely simulated, the simulated values becomes the conditioning data on the medium gird (b). Then using the medium (2nd) grid search template (e) to scan the medium grid (b), the black nodes on the medium grid are simulated, which turns into the conditioning data of fine (3rd) grid (c). (For interpretation of the references to colour in this figure legend, the reader is referred to the Web version of this article.)

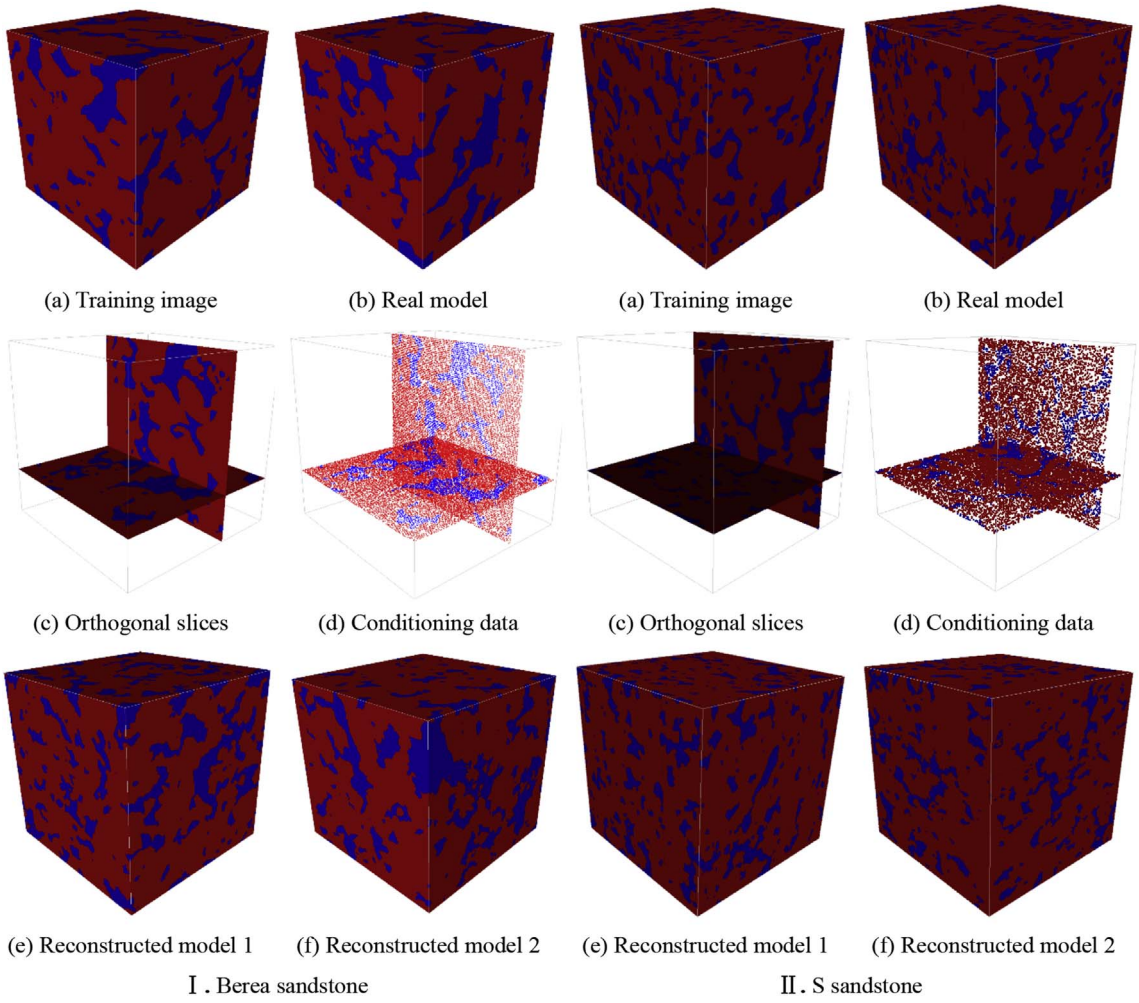

Fig. 5. The original images, conditioning data and reconstructed models of the Berea sandstone and S sandstone. The red represents particle and blue represents pore. (For interpretation of the references to colour in this figure legend, the reader is referred to the Web version of this article.)

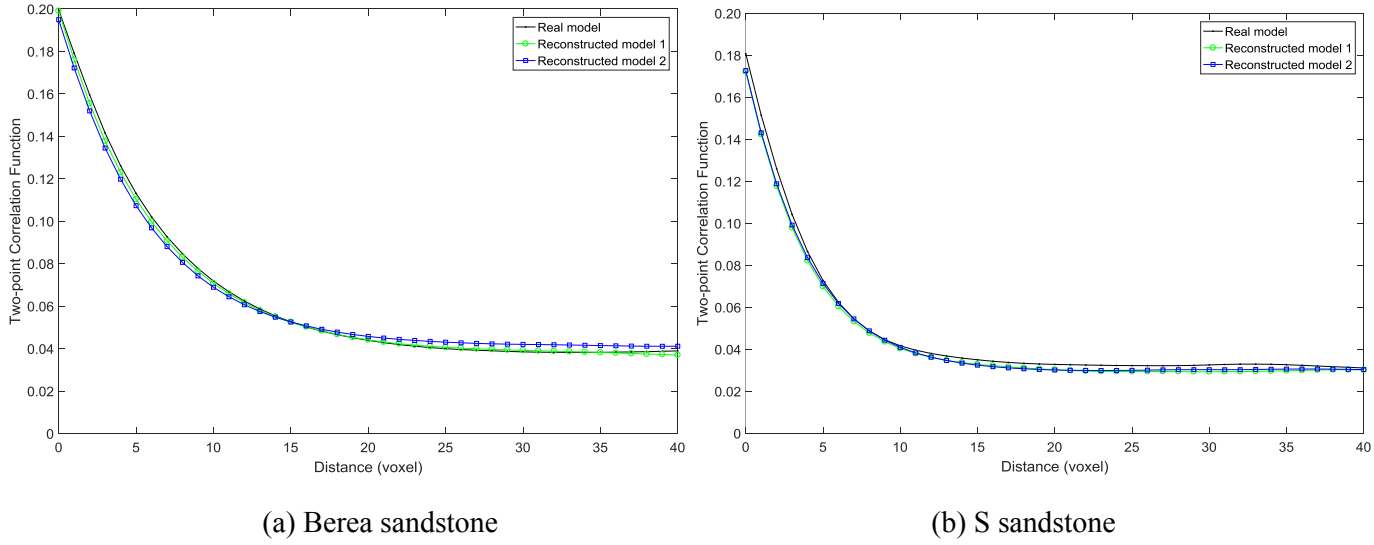

Fig. 6. Two-point correlation functions of the real model and the reconstructed models.

sample is more heterogeneous. Basic information on the Berea sandstone and S sandstone has been provided by Dong (2008) and Dong and Blunt (2009), where S sandstone corresponds to S3 sandstone. For each porous medium, two RVE of 150^3 voxels are extracted from different locations. One RVE is set as the training image in order to supply the 3D pore-space structure patterns (Fig. 5**Ⅰ**a and**Ⅱ**a). The other is taken out for providing the conditioning data and validating the accuracy of the next reconstructed porous media, so it is assumed as the real model in

Table 1
Pore space parameters of the real model and the reconstructed models for Berea sandstone and S sandstone.

Category		Porosity (%)	Connected volume ($\times 10^6 \mu m^3$)	Isolated volume ($\times 10^6 \mu m^3$)	Connectivity (%)	Centroid path tortuosity
Berea sandstone	Real model	19.95	100.0912	2.7246	97.35	1.91
	Reconstructed model 1	19.90	96.3739	6.1843	93.97	1.79
	Reconstructed model 2	19.49	93.2633	7.1818	92.85	1.93
S Sandstone	Real model	18.07	435.9559	23.6222	94.86	2.33
	Reconstructed model 1	17.22	406.9962	30.9635	92.93	2.55
	Reconstructed model 2	17.27	400.4853	38.7396	91.18	2.58

the paper (Fig. 5**I**b and**II**b). The porous media with the size of 150^3 voxels for the Berea sandstone and S sandstone will be reconstructed using SNESIM algorithm through the main steps as follows:

(1) First, the four multi-grid search template is used to scan the training image for the purpose of capturing multi-scale pore space structure patterns. Then a search tree is built for storing these patterns. With regard to the explanation, the four multi-grid template not only captures the scale of pore structure pattern, but it is also able to improve the modeling efficiency. In addition, the 3D training image is chosen so as to supply 3D pore space structure features. Moreover, in order to capture the large-scale pore structures, the search radius of the search template is set to $40 \times 40 \times 40$ and the search angles are set to 0°.
(2) Two orthogonal 2D slices (Fig. 5**I**c and**II**c) are chosen from the real model, the second RVE, as the known information. Some pixels from the two slices are extracted as the conditioning data (Fig. 5**I**d and**II**d). A random path is selected, and a voxel to be simulated is visited.
(3) Under the constraint of the conditioning data in the range of the maximal search template, simulate an unknown voxel. Assuming that the number of conditioning data is n and the corresponding data event is d_n, the CPDF of the data event will be retrieved form the search tree.
(4) A certain value of the central voxel **u** as the next conditioning data is randomly choose, and the other unknown voxels is simulated. The value of the central voxel can be one of two possible values, void space or solid.
(5) The third and fourth steps along the random path are repeated until all the unknown voxels are simulated.

Based on the aforementioned steps and parameter settings, the porous media with the size of 150^3 voxels for the Berea sandstone and S sandstone were generated, as shown in Fig. 5 (e) and (**f**). To guarantee generating the ideal results, some key parameters should be set appropriately, which is essential for building the accurate porous media. The target marginal distribution and servosystem factor can control the proportion of the pores and grains in the model to be simulated. Target marginal distribution is set to 0.2 for Berea sample and 0.17 for S sandstone and the servosystem factor is 0.9. Last but not least, with the purpose of reproducing the low proportional pore structure features for example too large pores or grains, the minimum number of training replicates is input to 1. The more detailed sensitive analyses of some key parameters used were given by Liu (2006).

4. Results and discussion

The accuracy of the proposed method is validated by comparing the two-point correlation function, the pore network structure parameters and the single-phase flow characteristic of the stochastic reconstructions with those of the real model.

4.1. Comparison on two-point correlation function

To reflect the spatial characteristics of the pore structures, two-point correlation function is introduced that is define as

$$S(\mathbf{x}, \mathbf{x}+\mathbf{h}) = \langle I(\mathbf{x}) I(\mathbf{x}+\mathbf{h}) \rangle \quad (2)$$

where $\mathbf{x}$ and $\mathbf{x} + \mathbf{h}$ are two arbitrary voxels in the 3D models. The $\mathbf{h}$ is the magnitude of the vector. I $I(\mathbf{x})$ is an indicate function. $I(\mathbf{x}) = 1$ when x is in the void space and $I(\mathbf{x}) = 0$ otherwise. $\langle I(\mathbf{x}) I(\mathbf{x}+\mathbf{h}) \rangle$ Represents the average of the multiplication of two indicator functions. So $S(\mathbf{x}, \mathbf{x}+\mathbf{h})$ can be interpreted as the probability of finding two voxels at different positions $\mathbf{x}$ and $\mathbf{x} + \mathbf{h}$ both in the pore space, which is a morphological descriptor of the pore structure of porous media (Yeong and Torquato, 1998). The two-point correlation function curves of the real model and the generated models for Berea sandstone and S sandstone are shown in Fig. 6. Each value of the curves is the average of the two-point correlation functions calculated in the X, Y and Z directions for each model. The comparison results show that the two-point correlation function curves are practically identical for Berea and S porous media.

4.2. Comparison on pore space

Porosity is the basic parameter to evaluate the accuracy of the pore space for a porous medium. The porosity of all the models is calculated in Table 1. Under the control of target marginal probability and servosystem, the porosity of the stochastic reconstructions is close to that of the real model regardless of the sample type, and the maximum gap is less than 1%. According to whether the pore space is connected or not, the pore space can be divided into invalid and valid pore space. Valid pore space means pore bodies are connected with other pore bodies by throats. Connectivity coefficient is used to represent pore-space connectivity. The bigger the connectivity coefficient, the better the connectivity. The calculation results show that the connectivity of stochastic reconstructions approximate the connectivity of the real model for each test sample. Besides, the connectivity algorithm can be applied to extract the connected pore space, and then the isolated pore space can be obtained by subtracting the connected pore space from total pore space. The pore space distributions of the real model and the reconstructed models are shown in Fig. 7. The isolated pore space of the generated models is only a small minority, which verifies that the reconstructed models have good connectivity. To contrast the complexity of the real model and reconstructed models, the centroid path tortuosity is introduced and it is defined as the ratio between actual path length of pore space along a direction and the distance of two centroids of the curved pore space. It is a parameter of characterizing the complex pore space. The greater the tortuosity value, the more complicated the pore structure is. As for the Berea sandstone, the values of the centroid path tortuosity are nearly 1.9 for the real porous medium and the generated porous media. The values approximate 2.5 for S sandstone.

4.3. Comparison on pore network structures

Because the spatial variation of complex pore structures cannot be characterized by only two-point correlation function, pore network structure parameters of these models are computed in order to further characterize the geometry and topology features of pore structures. At present, according to the extraction way of the pore network, the

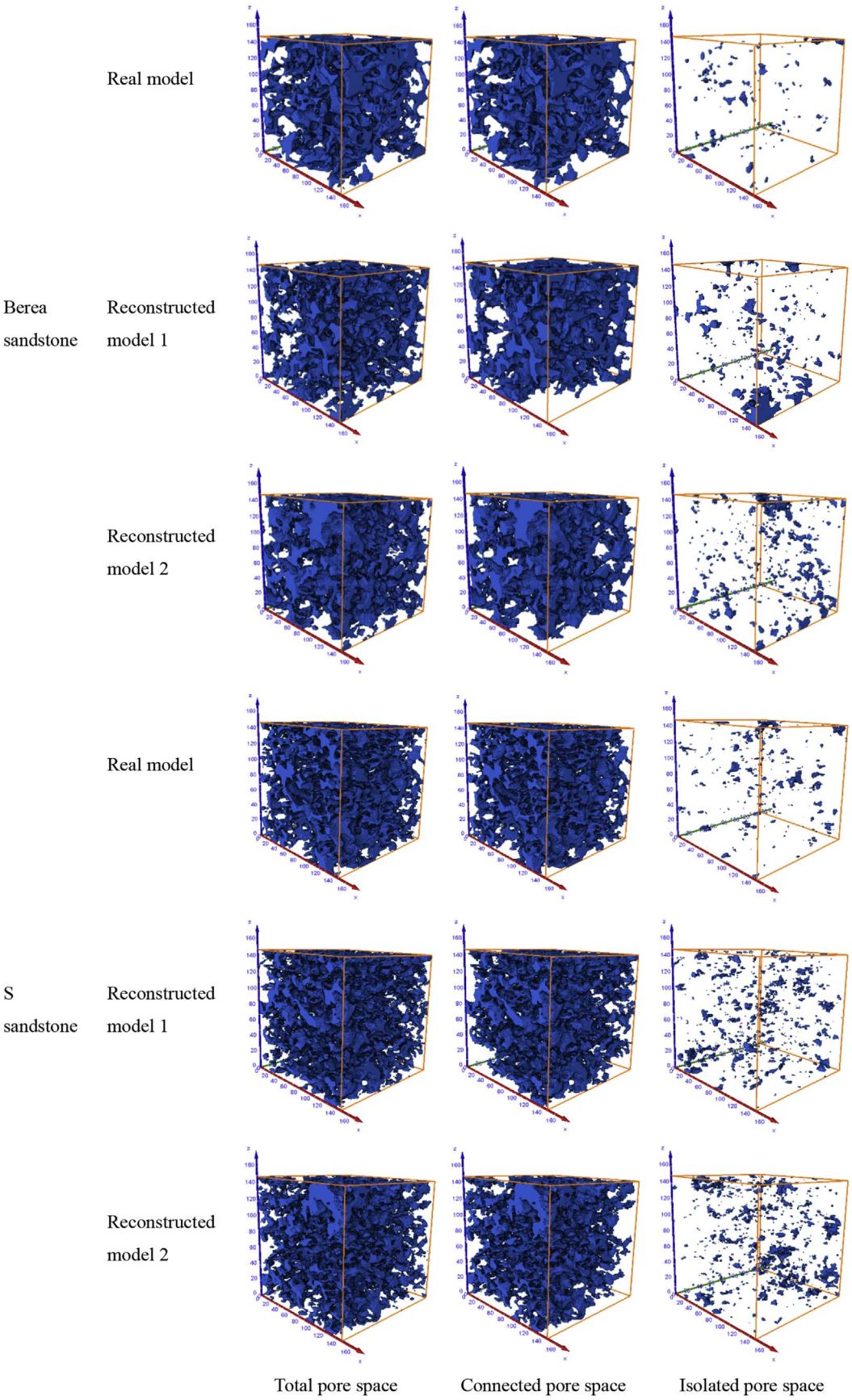

Fig. 7. Pore space of the real model and reconstructed models for Berea sandstone and S sandstone.

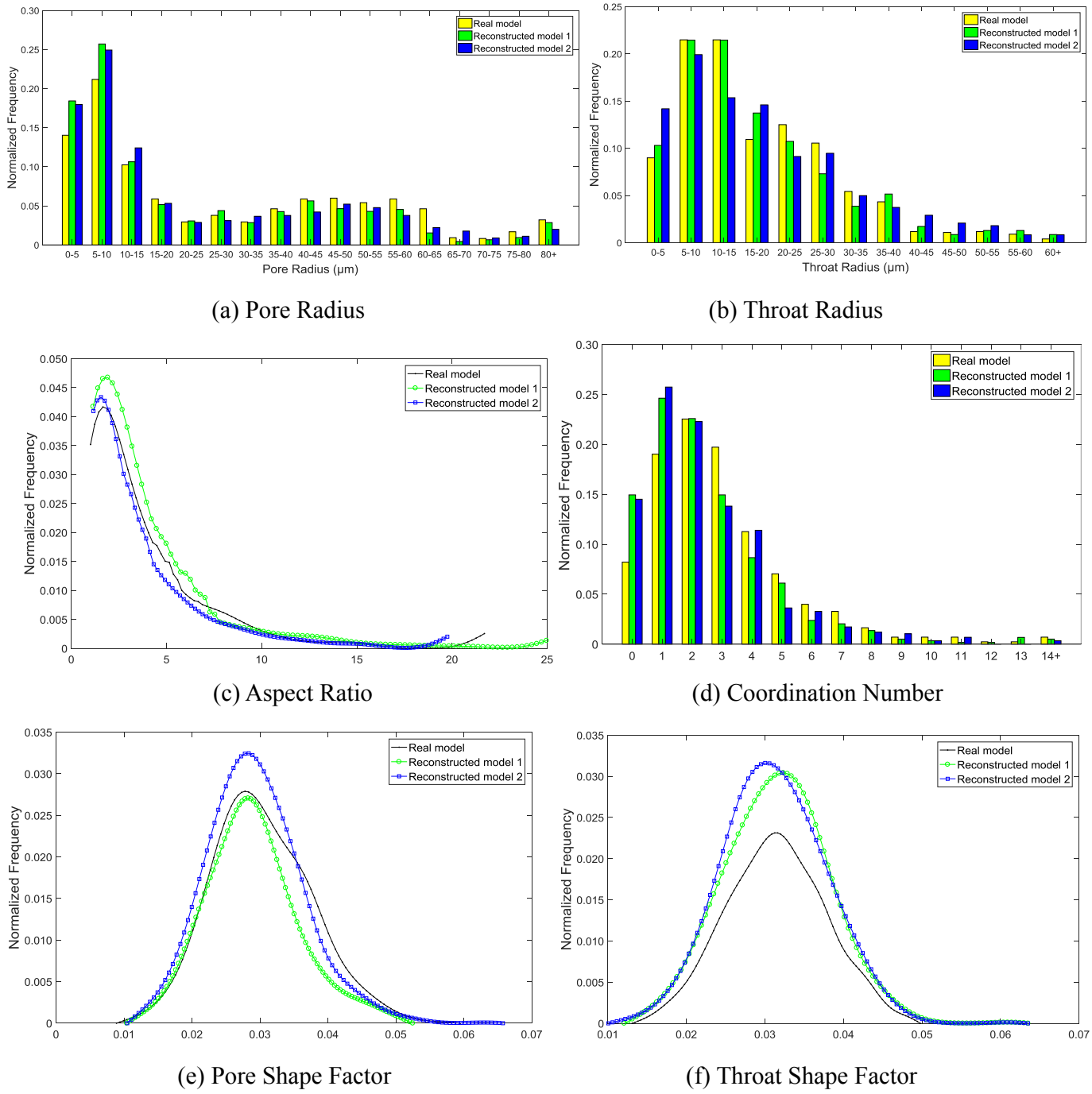

Fig. 8. Pore network structure parameter distributions of the real model and reconstructed models for Berea sandstone.

presented algorithms of extracting pore network mainly include multi-orientation scanning (Liang et al., 2000), the medial axis (Baldwin et al., 1996), Voronoi tessellation method (Bryant and Blunt, 1992) and the maximal ball method (Dong and Blunt, 2009).

In this paper, the pore network models of the real model and the stochastic models are extracted using the improved maximal ball method (Yan, 2013), and the accuracy of the reconstructed models is verified by comparing some pore structure geometry and topology parameters of the reconstructed models with those of the real model. First, it is necessary to briefly describe some key parameters. The aspect ratio means the ratio of the pore radius to the linked average value of all the throat radii. Shape factor is an important parameter to describe the shape of pore or throat cross section in porous media and is also an important factor affecting the fluid flow. The formula for calculating the shape factor G is as follow:

$$G = \frac{A}{P^2} \tag{3}$$

where A is the cross-sectional area of pore body or throat and P is the corresponding perimeter. The larger the shape factor G, the smoother the pore throat section is and the smaller the resistance to the fluid flow is.

The distributions of some pore network parameters including the pore and throat radius, pore throat ratio, pore and throat shape factor and coordination number are drawn (Figs. 8 and 9) in order to further assess the quality of the reconstructed models. More pores and throats with small radii are found in the stochastic reconstructions regardless of sandstone sample, but good agreement is acquired between the pore or

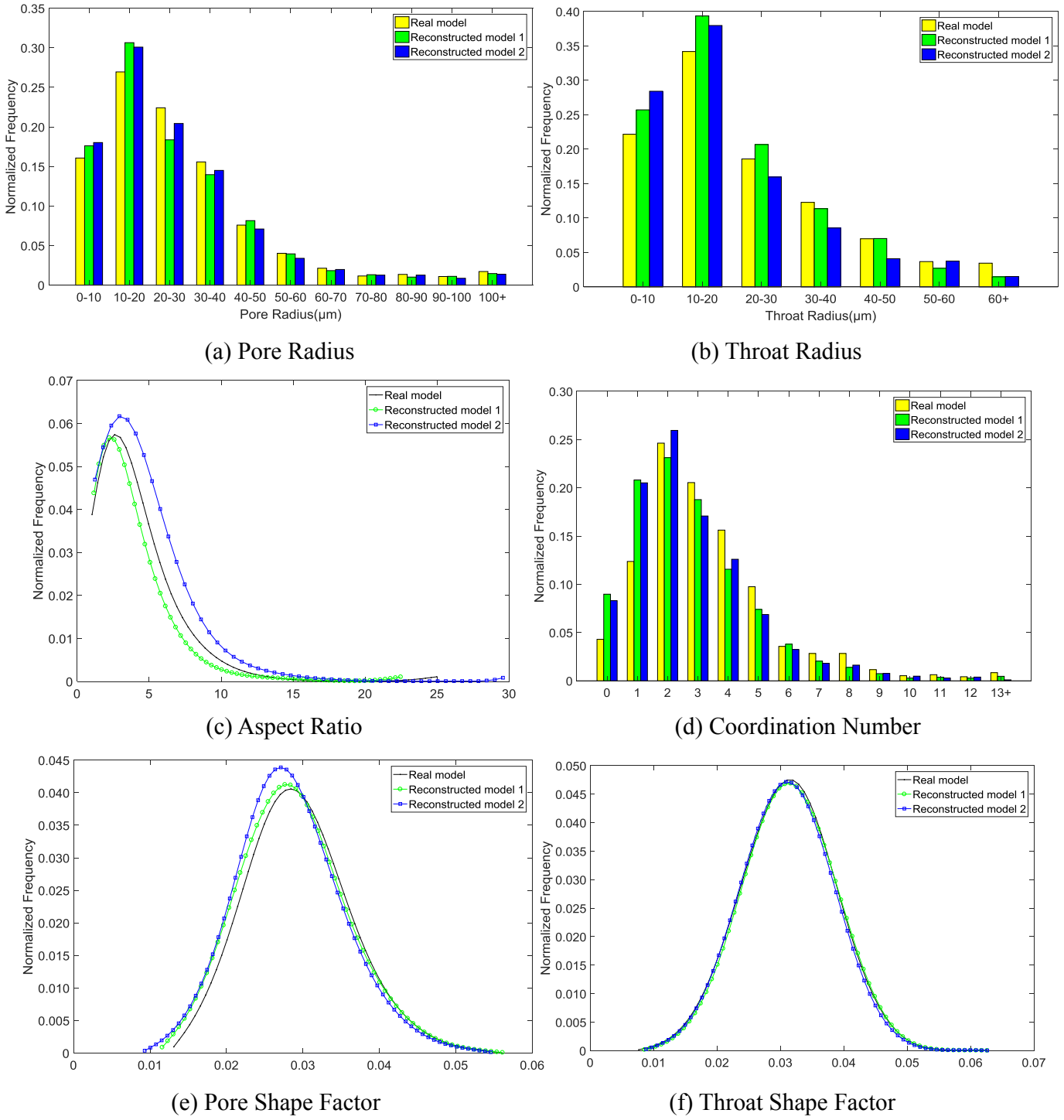

Fig. 9. Pore network structure parameter distributions of the real model and reconstructed models for S sandstone.

throat size distributions of the real image and reconstructed images. All the models show similar aspect ratios distributions in Figs. 8(c) and 9(c). Besides, the real and generated porous media of two samples give similar distributions of the coordination numbers although the real models define slightly higher coordination numbers (Figs. 8d and 9d). For the Berea sandstone, the pore shape factor distributions are similar even though the peak values of different images are different, so are the throat shape factor distributions in Fig. 8(e) and (f). The reconstructed models of S sandstone are in good agreement with the real model in the pore and throat shape factor distribution. The similar distribution of these pore network parameters further confirms the reliability of the reconstructed models and the presented method.

The pore network model can visually demonstrate the relation of pore throat spatial distribution and pore throat configuration. The improved maximal ball algorithm is used to extract the pore network models of the four models. Fig. 10 exhibits the pore network models of six porous media where the spheres represent pores and the tube columns represent throats. The larger the volume of the geometry, the greater the radius of the corresponding pore or throat is. A sphere connected by no column indicates that here the pore is an isolated pore, correspondingly with no coordination number. With regard to the real model and reconstructed models the for Berea and S sample, most of the

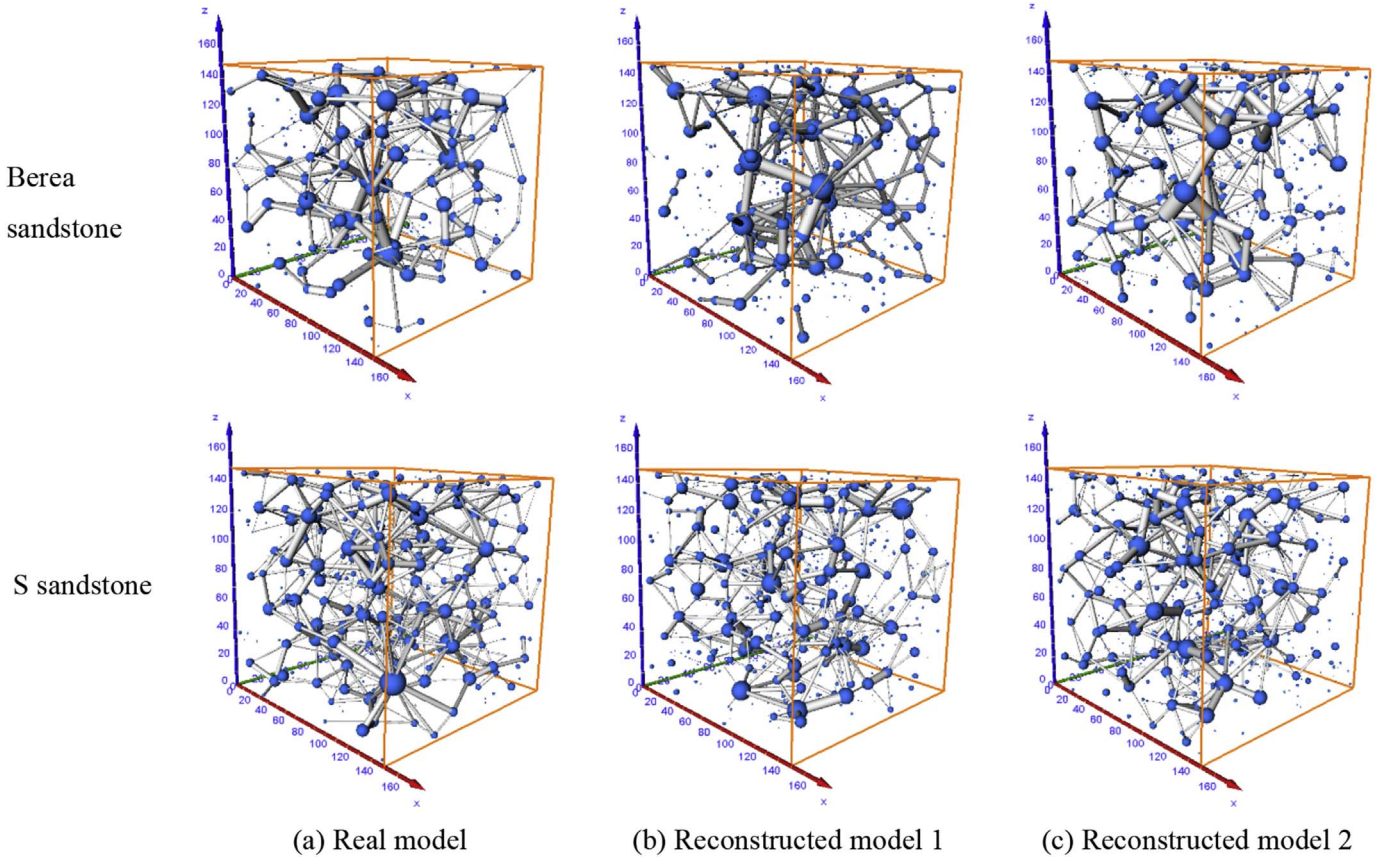

Fig. 10. Pore network models of the real model and reconstructed models for Berea sandstone and S sandstone.

Table 2
Absolute permeability of the real model and the reconstructed models for Berea sandstone and S sandstone.

Absolute permeability/ $\times 10^{-3}\mu m^2$	Experimental measure	Real model	Reconstructed model 1	Reconstructed model 2
Berea sandstone	1100	1032.56	986.96	975.27
S sandstone	109[a]	123.56	110.24	115.69

[a] The value is obtained from Dong and Blunt (2009), where S sandstone corresponds to S3 sandstone.

pores are connected by 2–4 throats. Overall, the pore throat configuration of the real model and the reconstructed models for two test samples is similar.

4.4. Comparison on absolute permeability

The numerical simulation experiment of single-phase flow is carried out on the basis of the real and reconstructed digital rocks. The flow process is steady-state. The fluid is an incompressible Newtonian fluid, and the fluid solid interface is no-slip. One end of the Z axis of the model is set as an inlet at a pressure of 130000Pa and the other end is an outlet with a pressure of 100000Pa. The fluid viscosity is set to 0.001Pa. S.

According to the experiment of single-phase fluid flow, the absolute permeability in the Z axis direction of the real model and the reconstructed models is calculated based on Navier-Stokes equation and Darcy's law, shown in Table 2. The numerical simulation values of these models approximate the experimentally measured absolute permeability, which further verifies the reliability of the reconstructed models. For the test samples, the permeability of the stochastic reconstructions is slightly smaller than that of the real model because the average coordination numbers in the reconstructed models are somewhat lower than those of the real model and the values of the centroid path tortuosity of the generated models are larger than ones of the real model.

5. Conclusions

Accurate porous medium is the basis of carrying out the petrophysics numerical experiment. In this paper, the method of reconstructing the digital rock model based on a 3D training image using multiple-point statistics was proposed. Two REV with 150^3 voxels are extracted from the digital rock established by X-ray computed tomography scanning. One REV is used as the 3D training image for supplying the 3D pore structure patterns, the other for providing the conditioning data and being the contrast model that is assumed as the real model. Two orthogonal 2D slices are chosen from the real model as the conditioning data. Then the porous media are reconstructed using SNESIM algorithm. A series of parameter comparisons including two-point correlation function, the pore network structure parameters and single-phase flow property have been made between the real model and reconstructed models. The comparisons results show that the good accuracy of the stochastic reconstructions and high reliability of the proposed method.

In terms of the application of the proposed method, as we know that the high cost of the micro-CT scan experiment makes it impossible that a large number of cores are scanned, so the presented technique in the paper provides a new idea for the reconstruction of porous media from the same geological background at a low cost. The reason is explained as follows. Supposing some core samples have the similar lithology and are from the same geological background including the diagenetic

processes and sedimentary facies, it can be believed that these cores have similar pore structure patterns. It is known that the pore space of the digital rock consists of different pore structure patterns, so the pore space is the result of the combinations of various pore structure patterns. A metaphor is made to further explain it, the pore space is like the sedimentary facies and a pore structure is equivalent to a sedimentary micro-facies. The sedimentary facies is composed of these micro-facies and the pore space has the same characteristic that many pore structures compose the pore space. So when only one core sample with micro-CT data is available, we can take this sample as the 3D training image to supply the pore structures for the purpose of reconstructing the digital rocks for other core samples without being scanned in the same geological background. The reconstructed porous media just borrow the pore structure patterns from the known sample with micro-CT data. Although the samples are from the same geological background, their pore space are somewhat different because the combinations and configurations of these pore structure patterns are diverse. So the proposed technique aims to reconstruct the porous media for similar cores from the same geological background when the micro-CT data of only one sample is available. There are several advantages of the method proposed. One is that a 3D training image as opposed to a 2D training image can provide more real 3D pore structure patterns, which ensures that good long-range connectivity of pore space can be generated in the reconstructed models. In addition, this statistical method is still suitable for moderately heterogeneous rocks, of which pore radii vary by 2–3 orders of magnitude. However, the shortcoming of the method is that it usually generates bad stochastic reconstructions when the samples have high heterogeneity, for example carbonate rocks with conventional pores, vugs and fractures, because some rare pore structure patterns in the porous media tend to occupy a small proportion and these rare structure patterns are difficult to be reproduced in the reconstructed model. Besides, the method is a bit computationally intensive. If the computer has higher CPU and larger memory, the larger-scale model can be reconstructed using multiple-point statistics. The larger digital rock model can be then taken as a platform for petrophysics experiment simulation, which is more significant for predicting the macroscopic transport properties in porous media.

Acknowledgments

This work was funded by Technology Major Project, P.R. China (grant number 2016ZX05054012) and the National Natural Science Foundation of China (grant numbers 41602135, 41672129). We would like to thank Branko Bijeljic from Imperial College London for providing the data of this research and Talemwa Emmanuel from China University of Petroleum (East China) for offering some useful advice.

Nomenclature

A	cross-sectional area
CPDF	conditional probability distribution function
d_n	data event
G	number of grid
G	shape factor
G^g	gth grid
H	distance of two nodes/voxels
$I(\mathbf{x})$	indicate function
MPS	multiple-point statistics
P	perimeter
N	total nodes number in data template except central node
SNESIM	single normal equation simulation
$S(x, x+h)$	two-point correlation function
u	central node of a search template
x	one voxel

Greek letter

α	sequence of vectors
τ_n	data template/search template
τ_n^g	gth grid search template

References

Abdelfatah, E., Pournik, M., Shiau, B.J.B., Harwell, J., 2017. Mathematical modeling and simulation of nanoparticles transport in heterogeneous porous media. J. Nat. Gas Sci. Eng. 40, 1–16.

Alizadeh, M., Moshirfarahi, M.M., Rasaie, M.R., 2014. Mathematical and neural network prediction model of three-phase immiscible recovery process in porous media. J. Nat. Gas Sci. Eng. 20, 292–311. https://doi.org/10.1016/j.jngse.2014.07.016.

An, S., Yao, J., Yang, Y., Zhang, L., Zhao, J., Li, A., 2016a. The microscale analysis of reverse displacement based on digital core. J. Nat. Gas Sci. Eng. https://doi.org/10.1016/j.jngse.2016.12.014.

An, S., Yao, J., Yang, Y., Zhang, L., Zhao, J., Gao, Y., 2016b. Influence of pore structure parameters on flow characteristics based on a digital rock and the pore network model. J. Nat. Gas Sci. Eng. 31, 156–163. https://doi.org/10.1016/j.jngse.2016.03.009.

Arabjamaloei, R., Ruth, D.W., 2016. Lattice Boltzmann based simulation of gas flow regimes in low permeability porous media: Klinkenberg's region and beyond. J. Nat. Gas Sci. Eng. 31, 405–416. https://doi.org/10.1016/j.jngse.2016.03.056.

Baldwin, C.A., Sederman, A.J., Mantle, M.D., Alexander, P., Gladden, L.F., 1996. Determination and characterization of the structure of a pore space from 3D volume images. J. Colloid Interface Sci. 181, 79–92. https://doi.org/10.1006/jcis.1996.0358.

Biswal, B., Øren, P.E., Held, R.J., Bakke, S., Hilfer, R., 2007. Stochastic multiscale model for carbonate rocks. Phys. Rev. E 75, 061303. https://doi.org/10.1103/physreve.75.061303.

Blunt, M.J., Bijeljic, B., Dong, H., Gharbi, O., Iglauer, S., Mostaghimi, P., Paluszny, A., Pentland, C., 2013. Pore-scale imaging and modelling. Adv. Water Resour. 51, 197–216. https://doi.org/10.1016/j.advwatres.2012.03.003.

Boucher, A., 2009. Considering complex training images with search tree partitioning. Comput. Geosci. 35, 1151–1158. https://doi.org/10.1016/j.cageo.2008.03.011.

Bryant, S., Blunt, M., 1992. Prediction of relative permeability in simple porous media. Phys. Rev. A 46, 2004–2011. https://doi.org/10.1103/physreva.46.2004.

Chen, X., Yao, G., 2017. An improved model for permeability estimation in low permeable porous media based on fractal geometry and modified Hagen-Poiseuille flow. Fuel 210, 748–757. https://doi.org/10.1016/j.fuel.2017.08.101.

Chen, X., Yao, G., Cai, J., Huang, Y., Yuan, X., 2016. Fractal and multifractal analysis of different hydraulic flow units based on micro-CT images. J. Nat. Gas Sci. Eng. 1–12. https://doi.org/10.1016/j.jngse.2016.11.048.

Chen, X., Zhou, Y., 2017. Applications of digital core analysis and hydraulic flow units in petrophysical characterization. Adv. Geo-Energy Res. 1, 18–30.

Comunian, A., Renard, P., Straubhaar, J., 2012. 3D multiple-point statistics simulation using 2D training images. Comput. Geosci. 40, 49–65.

Deutsch, C.V., 1992. Annealing Techniques Applied to Reservoir Modeling and the Integration of Geological and Engineering (Well Test) Data. Stanford University, Palo Alto.

Dong, H., 2008. Micro-CT Imaging and Pore Network Extraction. Imperial College London.

Dong, H., Blunt, M.J., 2009. Pore-network extraction from micro-computerized-tomography images. Phys. Rev. E - Stat. Nonlinear Soft Matter Phys. 80, 36307.

Fullwood, D.T., Niezgoda, S.R., Kalidindi, S.R., 2008. Microstructure reconstructions from 2-point statistics using phase-recovery algorithms. Acta Mater. 56, 942–948.

Guardiano, F.B., Srivastava, R.M., 1993. Multivariate Geostatistics: Beyond Bivariate Moments, vol. 5. pp. 133–144. https://doi.org/10.1007/978-94-011-1739-5_12.

Hasanabadi, A., Baniassadi, M., Abrinia, K., Safdari, M., Garmestani, H., 2016a. Efficient three-phase reconstruction of heterogeneous material from 2D cross-sections via phase-recovery algorithm. J. Microsc. 264, 384–393.

Hasanabadi, A., Baniassadi, M., Abrinia, K., Safdari, M., Garmestani, H., 2016b. 3D microstructural reconstruction of heterogeneous materials from 2D cross sections: a modified phase-recovery algorithm. Comput. Mater. Sci. 111, 107–115.

Hajizadeh, A., Safekordi, A., Farhadpour, F.A., 2011. A multiple-point statistics algorithm for 3D pore space reconstruction from 2D images. Adv. Water Resour. 34, 1256–1267. https://doi.org/10.1016/j.advwatres.2011.06.003.

Hemes, S., Desbois, G., Urai, J.L., Schröppel, B., Schwarz, J.O., 2015. Multi-scale characterization of porosity in Boom Clay (HADES-level, Mol, Belgium) using a combination of X-ray μ-CT, 2D BIB-SEM and FIB-SEM tomography. Microporous Mesoporous Mater. 208, 1–20. https://doi.org/10.1016/j.micromeso.2015.01.022.

Hurley, N.F., Zhao, W., Zhang, T., 2015. Multiscale Digital Rock Modeling for Reservoir Simulation U.S. Patent 9,134,457.

Ioannidis, M.A., Kwiecien, M.J., Chatzis, I., 1997. Electrical conductivity and percolation aspects of statistically homogeneous porous media. Transport Porous Media 29, 61–83.

Ju, Y., Zheng, J., Epstein, M., Sudak, L., Wang, J., Zhao, X., 2014. 3D numerical reconstruction of well-connected porous structure of rock using fractal algorithms. Comput. Meth. Appl. Mech. Eng. 279, 212–226.

Kainourgiakis, M.E., Kikkinides, E.S., Galani, A., Charalambopoulou, G.C., Stubos, A.K., 2005. Digitally reconstructed porous media: transport and sorption properties. Transport Porous Media 58, 43–62. https://doi.org/10.1007/1-4020-3604-3_4.

Kakouei, A., Vatani, A., Rasaei, M., Sedaee Sola, B., Moqtaderi, H., 2017. Cessation of

Darcy regime in gas flow through porous media using LBM: comparison of pressure gradient approaches. J. Nat. Gas Sci. Eng. 45, 693–705. https://doi.org/10.1016/j.jngse.2017.06.018.
Keehm, Y., 2003. Computational rock physics: transport properties in porous media and applications. https://doi.org/10.1007/978-94-017-1114-2.
Keehm, Y., Mukerji, T., Nur, M., 2004. Permeability prediction from thin sections: 3D reconstruction and Lattice-Boltzmann flow simulation. Geophys. Res. Lett. 31, L04606. https://doi.org/10.1029/2003gl018761.
Kim, C.S., Ahn, S.H., Jang, D.Y., 2012. Review: developments in micro/nanoscale fabrication by focused ion beams. Vacuum 86, 1014–1035. https://doi.org/10.1016/j.vacuum.2011.11.004.
Liang, Z., Ioannidis, M.A., Chatzis, I., 2000. Geometric and topological analysis of three-dimensional porous media: pore space partitioning based on morphological skeletonization. J. Colloid Interface Sci. 221, 13–24. https://doi.org/10.1006/jcis.1999.6559.
Liu, M., Shabaninejad, M., Mostaghimi, P., 2017. Impact of mineralogical heterogeneity on reactive transport modelling. Comput. Geosci. 104, 12–19. https://doi.org/10.1016/j.cageo.2017.03.020.
Liu, J., Pereira, G.G., Liu, Q., Regenauer-Lieb, K., 2016. Computational challenges in the analyses of petrophysics using microtomography and upscaling: a review. Comput. Geosci. 89, 107–117.
Liu, Y., 2006. Using the Snesim program for multiple-point statistical simulation. Comput. Geosci. 32, 1544–1563. https://doi.org/10.1016/j.cageo.2006.02.008.
Minsky, M., 2011. Memoir on inventing the confocal scanning microscope. Scanning 10, 128–138. https://doi.org/10.1117/12.2218302.4848650669001.
Nooruddin, H.A., Blunt, M.J., 2016. Analytical and numerical investigations of spontaneous imbibition in porous media. Water Resour. Res. 52, 7284–7310. https://doi.org/10.1002/2015wr018451.
Okabe, H., Blunt, M.J., 2004. Prediction of permeability for porous media reconstructed using multiple-point statistics. Phys. Rev. E - Stat. Nonlinear Soft Matter Phys. 70, 66135. https://doi.org/10.1103/physreve.70.066135.
Okabe, H., Blunt, M.J., 2005. Pore space reconstruction using multiple-point statistics. J. Petrol. Sci. Eng. 46, 121–137. https://doi.org/10.1016/j.petrol.2004.08.002.
Okabe, H., Blunt, M.J., 2007. Pore space reconstruction of vuggy carbonates using microtomography and multiple-point statistics. Water Resour. Res. 43, W12S02. https://doi.org/10.1029/2006wr005680.
Øren, P.L., Bakke, S., 2002. Process based reconstruction of sandstones and prediction of transport properties. Transport Porous Media 46, 311–343. https://doi.org/10.1007/bf00136822.
Øren, P., Bakke, S., 2003. Reconstruction of Berea sandstone and pore-scale modelling of wettability effects. J. Petrol. Sci. Eng. 39, 177–199. https://doi.org/10.1016/s0920-4105(03)00062-7.
Paddock, S.W., 2000. Principles and practices of laser scanning confocal microscopy. Mol. Biotechnol. 16, 127–149. https://doi.org/10.1385/mb:16:2:127.
Qajar, J., Arns, C.H., 2016. Characterization of reactive flow-induced evolution of carbonate rocks using digital core analysis- part 1: assessment of pore-scale mineral dissolution and deposition. J. Contam. Hydrol. 192, 60–86. https://doi.org/10.1016/j.jconhyd.2017.08.002.
Quiblier, J.A., 1984. A new three-dimensional modeling technique for studying porous media. J. Colloid Interface Sci. 98, 84–102. https://doi.org/10.1016/0021-9797(84)90481-8.
Srivastava, M., 1992. Iterative Methods for Spatial Simulation: Stanford Center for Reservoir Forecasting. Rep. No. 5. pp. 24.
Strebelle, S.B., 2000. Sequential Simulation Drawing Structures from Training Images (unpublished PhD Thesis). .
Strebelle, S.B., 2002. Conditional simulation of complex geological structures using multiple-point statistics. Math. Geol. 34, 1–21.
Tahmasebi, P., Sahimi, M., 2012. Reconstruction of three-dimensional porous media using a single thin section. Phys. Rev. E - Stat. Nonlinear Soft Matter Phys. 85, 66709. https://doi.org/10.1103/physreve.85.066709.
Tahmasebi, P., Hezarkhani, A., Sahimi, M., 2012. Multiple-point geostatistical modeling based on the cross-correlation functions. Comput. Geosci. 16, 779–797. https://doi.org/10.1007/s10596-012-9287-1.
Tahmasebi, P., Javadpour, F., Sahimi, M., 2015a. Multiscale and multiresolution modeling of shales and their flow and morphological properties. Sci. Rep. 5.
Tahmasebi, P., Javadpour, F., Sahimi, M., 2015b. Three-dimensional stochastic characterization of shale sem images. Transport Porous Media 110, 1–11.
Talukdar, M.S., Torsaeter, O., 2002. Stochastic Reconstruction, 3D Characterization and Network Modeling of Chalk 35. pp. 1–21. https://doi.org/10.1016/s0920-4105(02)00160-2.
Talukdar, M.S., Torsaeter, O., Howard, J.J., 2004. Stochastic reconstruction of chalk samples containing vuggy porosity using a conditional simulated annealing technique. Transport Porous Media 57, 1–15. https://doi.org/10.1023/b:tipm.0000032737.59531.cf.
Thovert, J.F., Adler, P.M., 2011. Grain reconstruction of porous media: application to a Bentheim sandstone. Phys. Rev. E - Stat. Nonlinear Soft Matter Phys. 83, 056116..
Van der Land, C., Wood, R., Wu, K., Van Dijke, M.I.J., Jiang, Z., Corbett, P.W.M., Couples, G., 2013. Modelling the permeability evolution of carbonate rocks. Mar. Petrol. Geol. 48, 1–7. https://doi.org/10.1016/j.marpetgeo.2013.07.006.
Vaz, A., Maffra, D., Carageorgos, T., Bedrikovetsky, P., 2016. Characterisation of formation damage during reactive flows in porous media. J. Nat. Gas Sci. Eng. 34, 1422–1433. https://doi.org/10.1016/j.jngse.2016.08.016.
Wang, M., Chen, S., 2007. Electroosmosis in homogeneously charged micro- and nanoscale random porous media. J. Colloid Interface Sci. 314, 264–273.
Wang, M., Wang, J., Pan, N., Chen, S., 2007. Mesoscopic predictions of the effective thermal conductivity for microscale random porous media. Phys. Rev. E 75, 036702.
Wu, K., Crawford, J.W., 2004. An efficient Markov chain model for the simulation of heterogeneous soil structure. Soil Sci. Soc. Am. J. 68, 346–351. https://doi.org/10.2136/sssaj2004.3460.
Wu, K., Van Dijke, M.I.J., Couples, G.D., Jiang, Z., Ma, J., Sorbie, K.S., Crawford, J., Young, I., Zhang, X., 2006. 3D stochastic modelling of heterogeneous porous media – applications to reservoir rocks. Transport Porous Media 65, 443–467. https://doi.org/10.1007/s11242-006-0006-z.
Xu, Z., Teng, Q., He, X., Yang, X., Li, Z., 2012. Multiple-point statistics method based on array structure for 3d reconstruction of Fontainebleau sandstone. J. Petrol. Sci. Eng. 100, 71–80.
Yeong, C.L., Torquato, S., 1998. Reconstructing random media. II. Three-dimensional media from two-dimensional cuts. Phys. Rev. E 58, 224. https://doi.org/10.1103/physreve.58.224.
Yan, G., 2013. Research of Permeability Models of Reservoirs Based on Digital Cores. China University of Petroleum, Qingdao.
Zhang, T., 2015. MPS-driven digital rock modeling and upscaling. Math. Geosci. 47, 937–954. https://doi.org/10.1007/s11004-015-9582-1.